UNIVERSITY OF BIRMINGHAM
University of Birmingham Research at Birmingham

On the effect of crosswinds on the slipstream of a freight train and associated effects

Flynn, Dominic; Hemida, Hassan; Baker, Chris

DOI:
10.1016/j.jweia.2016.07.001

License:
Creative Commons: Attribution-NonCommercial-NoDerivs (CC BY-NC-ND)

Document Version
Peer reviewed version

Citation for published version (Harvard):
Flynn, D, Hemida, H & Baker, C 2016, 'On the effect of crosswinds on the slipstream of a freight train and associated effects', *Journal of Wind Engineering and Industrial Aerodynamics*, vol. 156, pp. 14-28. https://doi.org/10.1016/j.jweia.2016.07.001

Link to publication on Research at Birmingham portal

Publisher Rights Statement:
Checked 12/08/2016

General rights
Unless a licence is specified above, all rights (including copyright and moral rights) in this document are retained by the authors and/or the copyright holders. The express permission of the copyright holder must be obtained for any use of this material other than for purposes permitted by law.

•Users may freely distribute the URL that is used to identify this publication.
•Users may download and/or print one copy of the publication from the University of Birmingham research portal for the purpose of private study or non-commercial research.
•User may use extracts from the document in line with the concept of 'fair dealing' under the Copyright, Designs and Patents Act 1988 (?)
•Users may not further distribute the material nor use it for the purposes of commercial gain.

Where a licence is displayed above, please note the terms and conditions of the licence govern your use of this document.

When citing, please reference the published version.

Take down policy
While the University of Birmingham exercises care and attention in making items available there are rare occasions when an item has been uploaded in error or has been deemed to be commercially or otherwise sensitive.

If you believe that this is the case for this document, please contact UBIRA@lists.bham.ac.uk providing details and we will remove access to the work immediately and investigate.

Download date: 20. Aug. 2024

On the effect of crosswinds on the slipstream of a freight train and associated effects: a numerical investigation

Dominic Flynn*, Hassan Hemida & Chris Baker

Centre for Railway Research and Education, School of Civil Engineering, University of Birmingham, Edgbaston, Birmingham, UK, B15 2TT

*Corresponding author e-mail: D.C.Flynn@bham.ac.uk
Tel: +44 0121 4147971

Abstract

When a train moves through the air, a region of air moves along with it at approximately the same speed: this region of air is known as the 'slipstream'. Numerical simulations were conducted in order to simulate the slipstream around a model-scale freight train when subjected to crosswinds with two different yaw angles; 10° and 30°, and the results were compared to a previous slipstream study without a crosswind. The velocities on the windward side of the train for each case are generally lower than the crosswind speed due to the flow stagnation on the side of the train producing lower velocities than the no-crosswind case. On the leeward side, velocities from the 30° crosswind case remain higher than train speed for more than two metres from train side. Peak instantaneous velocities showed strong dependence on yaw angle and position from train side, and exhibiting superficial comparison to full-scale data. Velocities were used as inputs to a spring-mass-damper model which modelled human responses to wind gusts. It was shown that the effect of a crosswind on the train's slipstream causes a significant increase in the likelihood of a person becoming unsteadied while standing on the leeward side of the train.

Key words: Freight train, slipstream, computational fluid dynamics (CFD), numerical simulation, delayed detached-eddy simulation (DDES), crosswinds, person stability, mathematical model.

1. Introduction

When a train moves through the air it generates a slipstream which to a static observer appears as a gradually-building gust punctuated by pressure and velocity transients. The concept of a slipstream is well known by the general public and is colloquially referred to as ‘air turbulence’. In recent years, the drive for faster trains has led to an increased risk of person instability because slipstream velocities increase approximately with train speed and hence faster trains produce higher slipstream velocities. Considering that the force experienced by an object subjected to a wind increases nearly proportionally with the square of the velocity, any increase in train speed can significantly increase the forces experienced by a person in close proximity to a train.

The study of train slipstreams has largely been directed towards high speed passenger trains (Baker et al., 2001, Hemida et al., 2012, Muld et al., 2013, Bell et al., 2014, Huang et al., 2014), although these vehicles are generally very streamlined to reduce drag and hence the amount air which is locally deformed when the train passes through it is minimised. The contrary is the true for freight trains where geometries are generally bluffer making them responsible for thicker slipstreams and thus higher slipstream velocities are obtained than would be obtained from faster-moving passenger trains at the same distances from train side (Pope, 2006, Sterling et al., 2008).

Reports documenting the effect of train slipstreams on trackside infrastructure, people and objects on platforms, on the UK rail network over a three decade period (from 1972 to 2005) showed that train slipstreams have the potential to pose a safety threat (Pope, 2006). Documented incidents include empty pushchairs being moved into passing trains causing them to be destroyed and on one occasion a person’s jacket was caught by the slipstream of a passing train and the person was subsequently spun around. These

incidents are fairly minor and so far there have been no fatalities on the UK rail network. However more recently, two infant fatalities occurred in Switzerland and Austria where unattended pushchairs were drawn into the path of freight trains passing through stations (Bowman, 2015, Tages Anzeiger, 2015). The incidents highlight the risks associated with freight train slipstreams and objects on station platforms.

Full-scale data suggest that when train slipstreams are subjected to ambient winds velocities increase on the leeward side of the train. These velocity increases are hypothesised to be a result of slipstream convection toward the leeward side of the train (Baker et al., 2007, Quinn et al., 2011, Baker et al., 2013a, Baker et al., 2013b). The increased slipstream velocity observed in the presence of a crosswind is known as slipstream amplification. The rate of increase in slipstream velocities with resultant yaw angle (the relative angle between the wind and the train) has been shown to be greater for freight trains than for passenger trains (Baker et al., 2007) although due to the scarcity of this data the effects of crosswinds on the slipstreams of freight trains at full-scale is poorly understood.

A recent study by Baker et al., (2013a) and (2013b) showed that even at yaw angles less than $\theta=\pm1.5°$ a high speed passenger train's slipstream was affected by the relatively low-speed crosswinds. The two most prominent methods of data analysis in the field of train aerodynamics are ensemble-averaging and peak one-second moving averages. Ensemble averaging is the process of obtaining multiple velocity or pressure time series and aligning them about a characteristic feature and performing the average at positions along the train (Deeg et al., 2008). The peak one-second moving average is performed by applying a one-second average to the velocity and pressure time series for each run, and taking the peak values. The effect of the crosswinds were shown to be significant

for both ensemble-averages and peak one second moving-average velocities (Baker et al., 2013a, 2013b).

Under the current TSI (2008) regulations, the guidelines which specify limiting values for pressures and velocities in the slipstreams of trains, there are no limits for the slipstream velocities which a freight train can generate. This is due to the fact that freight trains generally travel below the minimum train speed considered in the regulations which is 160 km/h (44.4 m/s). Recent work by (Soper et al., 2014) has shown that the slipstream velocities produced by some freight trains with low loading efficiencies i.e. carrying smaller containers than the wagon length, border on the maximum values allowed for high speed passenger trains.

Considering the available data on slipstream behaviour in crosswinds it is anticipated that the TSI limits could be violated by a freight train during even moderate ambient wind conditions (Baker et al., 2007, Quinn et al., 2011, Baker et al., 2013a, Baker et al., 2013b). Therefore, to ensure safe operation of freight trains the effect of slipstream amplification needs to be properly understood in order to determine the risk associated with it and recommend any appropriate measures.

Investigating how crosswinds would affect freight train slipstreams is difficult to achieve at full-scale because of the variability of ambient winds as well as the number of freight train geometries in operation. Therefore obtaining sufficient data to provide meaningful results would require lengthy measurement campaigns to obtain any useful amount of data. Approaches such as numerical and physical modelling offer controlled environments in which to carry out such experiments. Physical modelling such as wind tunnel (Bell et al., 2014) and moving model (Soper et al., 2014, Bell et al., 2015) testing

allow for data to be collected relatively quickly and cheaply in comparison to full-scale data, although obtaining large data sets can prove arduous.

Numerical modelling has the main advantage of providing large amounts of data from a single simulation which would otherwise require lengthy physical experiments to obtain. However, instantaneous simulation methods such as large-eddy simulation (LES) that are capable of capturing the instantaneous slipstream characteristics come at a significant computational cost compared to steady methods which are cheaper but fail to provide such data. Numerical simulations have proved an effective tool for crosswind assessment (Diedrichs, 2003, Diedrichs et al., 2007, Bouferrouk et al., 2012, Golovanevskiy et al., 2012) and calculation of train slipstreams (Hemida and Krajnovic, 2005, Hemida and Baker, 2010, Hemida et al., 2012, Flynn et al., 2014, Huang et al., 2014, Pii et al., 2014). This being said, numerical simulations must be validated against physical experiments in order to prove that the numerical model produces physical results and therefore numerical and physical modelling are most effective when used in unison.

The current available literature shows that freight trains produce larger slipstream velocities than passenger trains for a given train speed. It is also known from full-scale experiments that the rate of increase of slipstream velocity with yaw angle is greater for freight trains rather than for passenger trains (Baker et al., 2007); however the data on this subject are relatively limited. Therefore to expand on the existing knowledge base and clarify the effect of crosswinds on freight train slipstreams and associated effects, a numerical investigation was conducted.

The present work uses delayed detached-eddy simulation (DDES) to simulate the flow around a $1/25^{th}$ scale Class 66 locomotive container-hauled freight train being subjected

to a 10^{o} and a 30^{o} crosswind. The primary goal of the research is to determine the effect of the crosswind on the train's slipstream. This work includes results from a previous freight train slipstream study (Flynn et al., 2014) and validation against previously conducted physical experiments (Soper, 2014) gives assurance of the simulations' physicality. The effect of crosswinds on the train's slipstream are investigated in terms of person stability using a previously-developed mathematical model (Jordan et al., 2008).

The layout of the present paper is as follows. Section 2 describes the model, section 3 contains a description of the computational domain and boundary conditions and section 4 describes the numerical method. Section 5 discusses the computational mesh and slipstream time-averaged and instantaneous results are presented in section 6. The description of the spring-mass damper model and results are contained in section 7 and conclusions are drawn and recommendations for future work are made in section 8.

2. Model description

The freight train used in the present work is a 1/25th scale Class 66 locomotive and 4 fully-loaded FEA type B container wagons; rails were also included in the simulations.

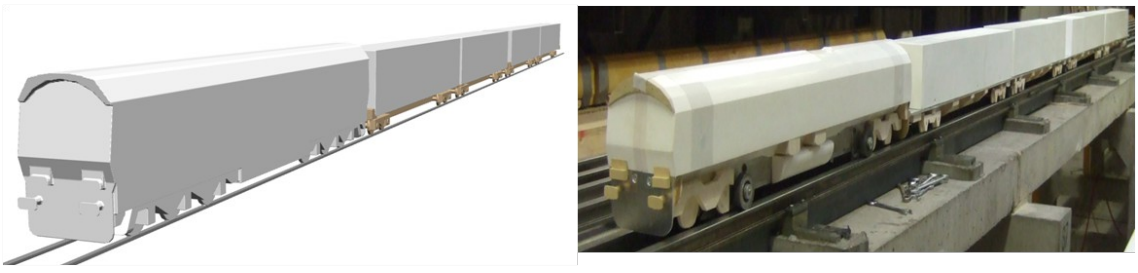

Figure 1 Models used in numerical (left) and physical experiments (right) (Soper, 2014)

Figure 1 shows the computer-aided design (CAD) model used in the numerical work and the physical model used in Soper et al., (2014). The majority of the important

external dimensions are exactly reproduced although minor geometrical features have been omitted from the CAD model to allow for higher mesh quality and thus a more accurate solution.

The dimensions presented in this paper are given as full-scale values to allow for ease of comparison to the real world. The locomotive has a full-scale height of 4.35 m, width of 2.35 m, the wheels are 1.20 m apart (where standard gauge is 1.435 m) and the lowest point of clearance between the train and the ground is 0.25 m (Figure 2). The dimensions of the CAD model relate to the physical model whose geometry was subject to the moving-model rig and do not necessarily compare to the full-scale vehicle. Longitudinal (*x*), lateral (y) and vertical (z) distances will be given relative to the front face of the locomotive, the centre of track and the top of rail, respectively. Positions relative to train side are given as y'.

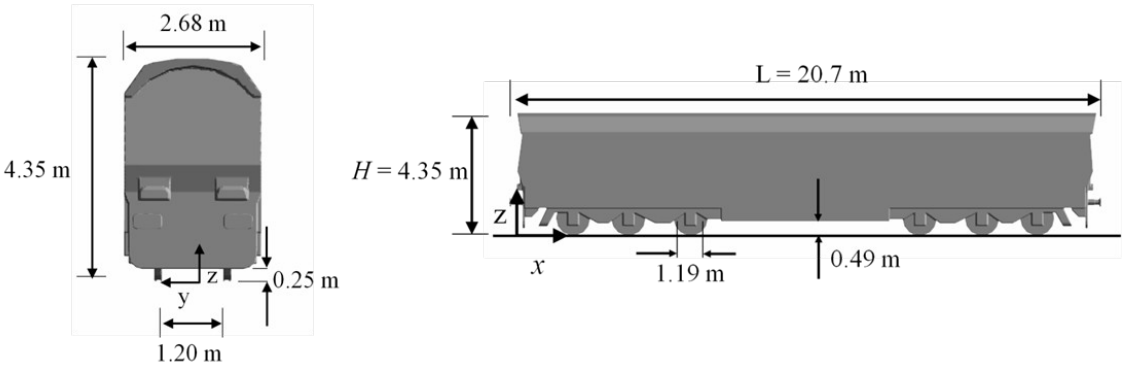

Figure 2 Dimensions of Class 66 locomotive

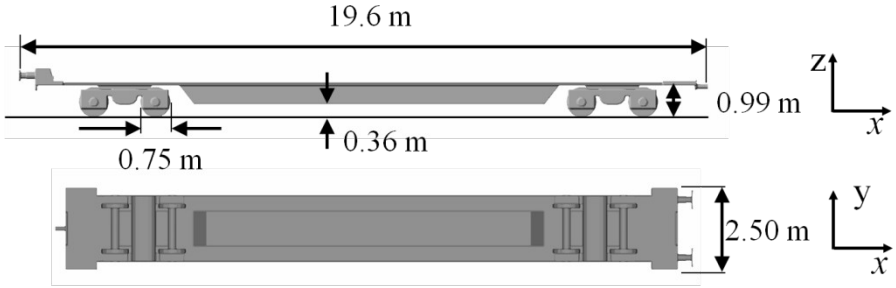

Figure 3 Side and plan views of the container flat

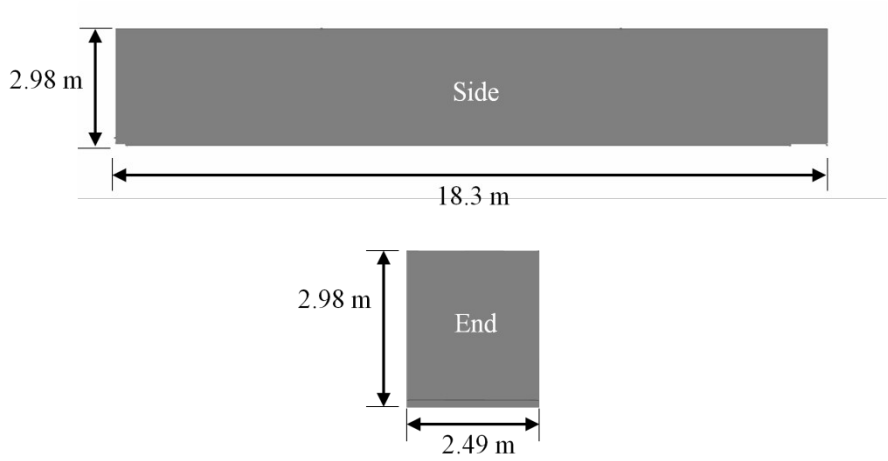

Figure 4 Shipping container dimensions

Each wagon consists of a container flat (Figure 3) and a representative shipping container (Figure 4). The container used on the wagons is a cuboid with external measurements of a standard 60 foot (18.3 m) shipping container and were simplified by neglecting the corrugations. This simplification was also made by Alam and Watkins (2007), Soper et al.,(2014) and Hemida and Baker (2010) and although the effect of neglecting the corrugations was not tested by either study the effect is assumed to be negligible due to their small size relative to other geometrical features. The total height of a container wagon is 4 m above TOR.

3. Computational domain and boundary conditions

The computational domain used in the present work is shown in Figure 5. The inlets provide a steady, uniform block velocity profile which give yaw angles of 10° and 30° where the resultant inlet velocity, u_r, is 23 m/s. Unlike The train is kept fixed and the ground plane is a no-slip moving wall and is set to the longitudinal inlet velocity component, u_{train}, which is also the train speed. This way the movement of a train can be simply replicated without the need for complicated methods such as sliding meshes. The outlets are zero-pressure outlets and the roof is set as a slip wall. The Reynolds

numbers (Re) of the simulations are 300,000, based on the height of the locomotive (H) and u_r.

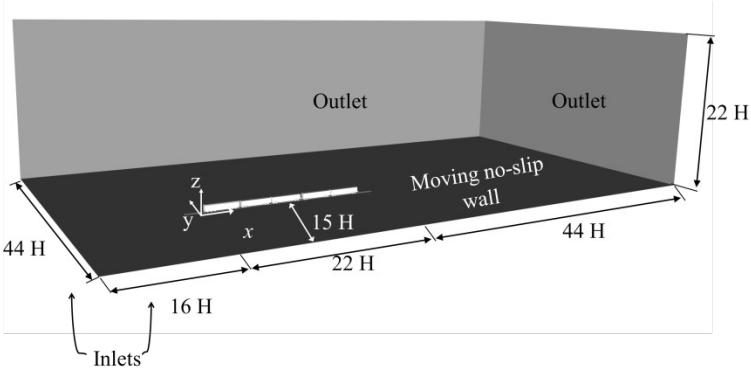

Figure 5 Computational domain used for the 10° and 30° crosswind simulations

The numerical simulations are designed to adhere as closely as reasonably possible to the crosswind experiments which they are validated against (Soper, 2014) although features such as the turbulence inlet characteristics are not considered. The TRAIN rig's crosswind generator (CWG) has an average turbulence intensity of approximately 15%, therefore the steady block profile inlet is a simplification of the actual case. Some turbulence at the inlet may be beneficial to the accuracy of the simulations but a steady inlet is specified to provide a baseline case and for simplicity.

4. Numerical method

The present work uses delayed detached-eddy simulation (DDES) in order to gain an instantaneous and an accurate time-averaged view of the slipstream around the freight train. The principle of DDES is that the attached flow on the wall is simulated using a RANS model whereas the detached flow is resolved using large-eddy simulation (LES). Using wall-resolved LES can be very computationally expensive in comparison to methods such as DDES, especially at higher Reynolds numbers, Re, where the computational cost of resolving the boundary layer can increase proportionally with

$Re^{1.8}$ (Piomelli, 2008). The Spalart-Allmaras one equation turbulence model was chosen because of the reduced computational cost required to solve it in comparison to commonly-used two equation models such as the k-ε or k-ω.

The diffusive and sub-grid fluxes were discretised using a second order central-differencing scheme. The convective term was discretised using central-differencing with a Sweby limiter (Sweby, 1984) to form a total variation diminishing (TVD) scheme; the limiter was set to $\Psi=0.6$ which provided a balance between stability and accuracy. Time integration was conducted using a second order backward implicit scheme and the maximum Courant-Friedrichs-Lewy (CFL) number was kept below 4 in all cells within the domain and the CFL number exceeds one in less than 1% of the cells and is therefore unlikely to have a significant effect on the flow.

Time-averaging of pressure and velocity was commenced once the flow was fully-developed which was determined by examining the moment coefficients on each wagon and container because they are generally more sensitive than force coefficients as the distance from the origin accentuates any imbalance in local frictional forces or surface pressures. Sampling probes placed near the inter-wagon spacings of the train were also used to confirm that the flow was fully-developed. Time-averaging was conducted for the time required for the flow to travel the length of a wagon 20 times, giving an equivalent full-scale time of 12 s which ensured that the motion of the lower-frequency turbulent fluctuations were incorporated in the average.

5. Computational mesh

The computational meshes used in the present work were unstructured hexahedral grids (Figure 6). The same meshes were used for the 10° and 30° crosswind cases which negated the process of further mesh generation which is advantageous for complex

geometries where quality mesh generation can be very time-consuming. Another advantage of using the same meshes for both crosswind cases is that there is no difference in mesh quality between the simulations. However, there is some drawback in terms of the additional cells required in the mesh. The coarse and fine meshes consisted of $45x10^6$ and $65x10^6$ cells, respectively, and the fine surface mesh consisted of approximately $8.4x10^5$ cells on each container wagon and $1x10^6$ cells on the locomotive.

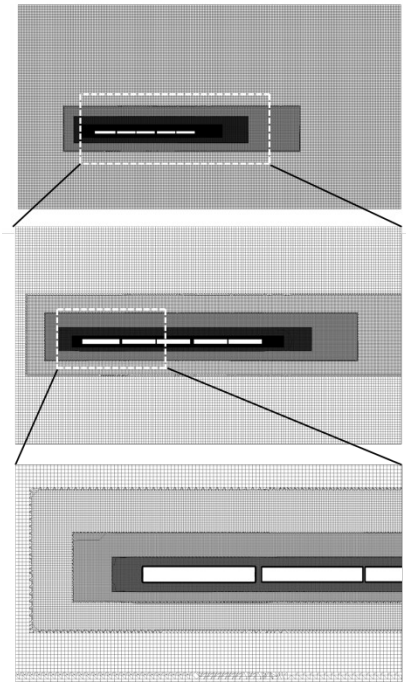

Figure 6 Computational mesh in crosswind cases on a plane at z=2 m.

The meshes are dominated by hexahedral cells but other polyhedral elements were also present due to the complexity of the geometry (Figure 7). The unstructured meshes were generated using SnappyHexMesh which is a utility within OpenFOAM. The quality of the meshes was verified using OpenFOAM's inbuilt mesh metrics and it was ensured that the maximum skewness of every cell was below 4 and maximum non-orthogonality was less than 60: corrections were made for the non-orthogonality in the solver.

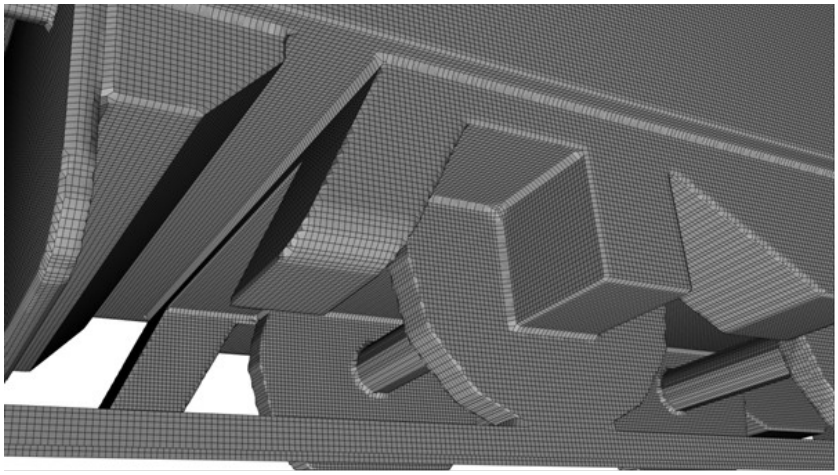

Figure 7 Surface mesh on the under-body region of locomotive

To ensure that the velocity gradients near the wall were correctly represented four prism layer cells were applied to the surface of the vehicle. The y^+ over the majority of the train's surface is between 10 and 50, with a small number of localised exceptions occurring. The Spalding wall function was applied because of the value of the average y^+ on the surface of the train. The maximum distance between the centre of the first cell and the surface of the train is 0.1 mm.

6. Results

6.1 Mesh sensitivity

Mesh sensitivity testing was conducted in order to determine whether the solutions are a function of mesh density. The time-averaged surface pressure coefficients, C_p, from the middle of each container, for the coarse and fine meshes, in the 30° case, are shown in Figure 8. The pressure coefficient, C_p, is calculated by

$$C_p = \frac{2p - p_\infty}{\rho u_r^2} \quad (1)$$

where p is the local mean static pressure, ρ is air density and p_∞ is the freestream pressure. In incompressible numerical simulations, pressure is considered as a gauge

value unlike physical experiments where the local atmospheric pressure must be taken into account, to this end we can consider p_∞ to be zero. The agreement between the pressure coefficients on the surface of each container is generally good, however some minor differences occur on the roofs of the first and second container wagons. The agreement between the results from the two mesh densities indicates that the energy-containing eddies have been resolved and that a finer mesh is not required. Mesh sensitivity testing was also conducted for the 10° case and showed nearly identical agreement between the fine and coarse meshes, although for conciseness the figure has been omitted here.

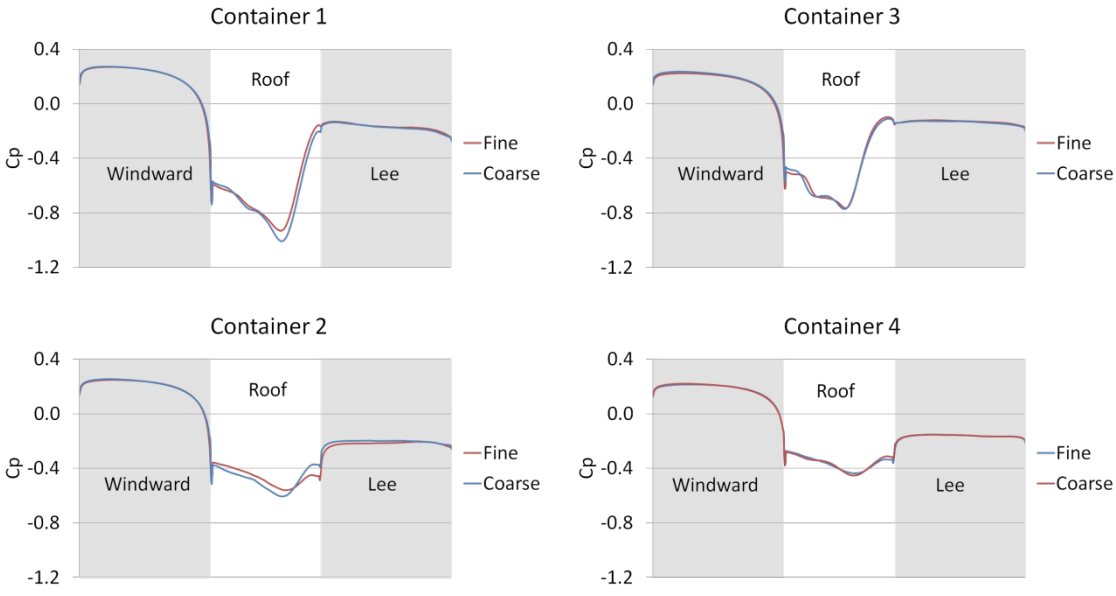

Figure 8 Surface pressure coefficients around each container at their mid-length for fine (blue) and coarse (red) meshes from the 30° crosswind case.

6.2 Validation

In order to ensure the physicality of the simulations, the results from the 30° crosswind simulations were validated against experimental data from Soper (2014). The experimental surface pressures were obtained by tapping only the third container in the train and ensemble-averaged over 15 runs. The locations of the pressure-taps on the surface of the third container are shown in Figure 9. The lateral and vertical taps were

made at 25%, 50% and 75% of the container width and height, respectively. The longitudinal taps were made at 16.6%, 33.3%, 50%, 66.6% and 83.3% along the length of the container. Further details of the experimental procedure can be found in (Soper, 2014).

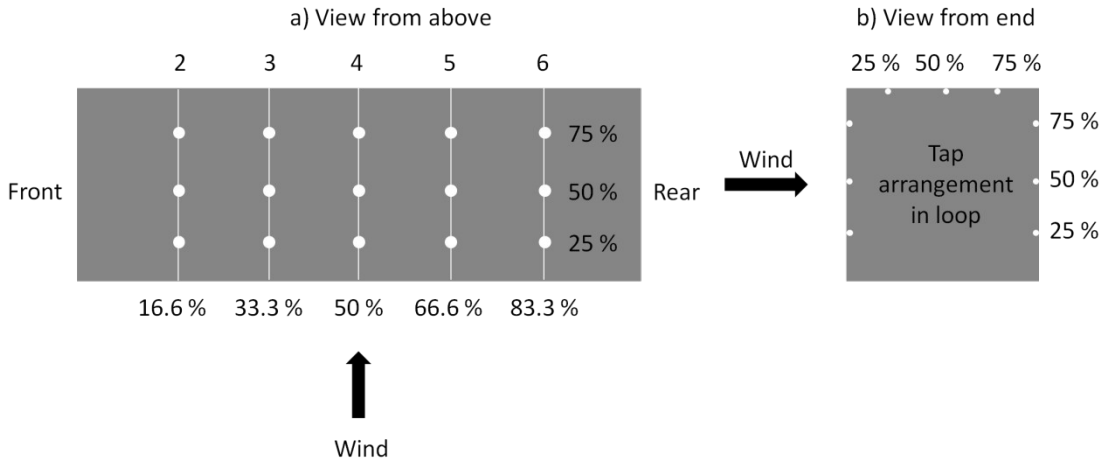

Figure 9 Positions of pressure taps on the a) roof and b) around the edges of third container

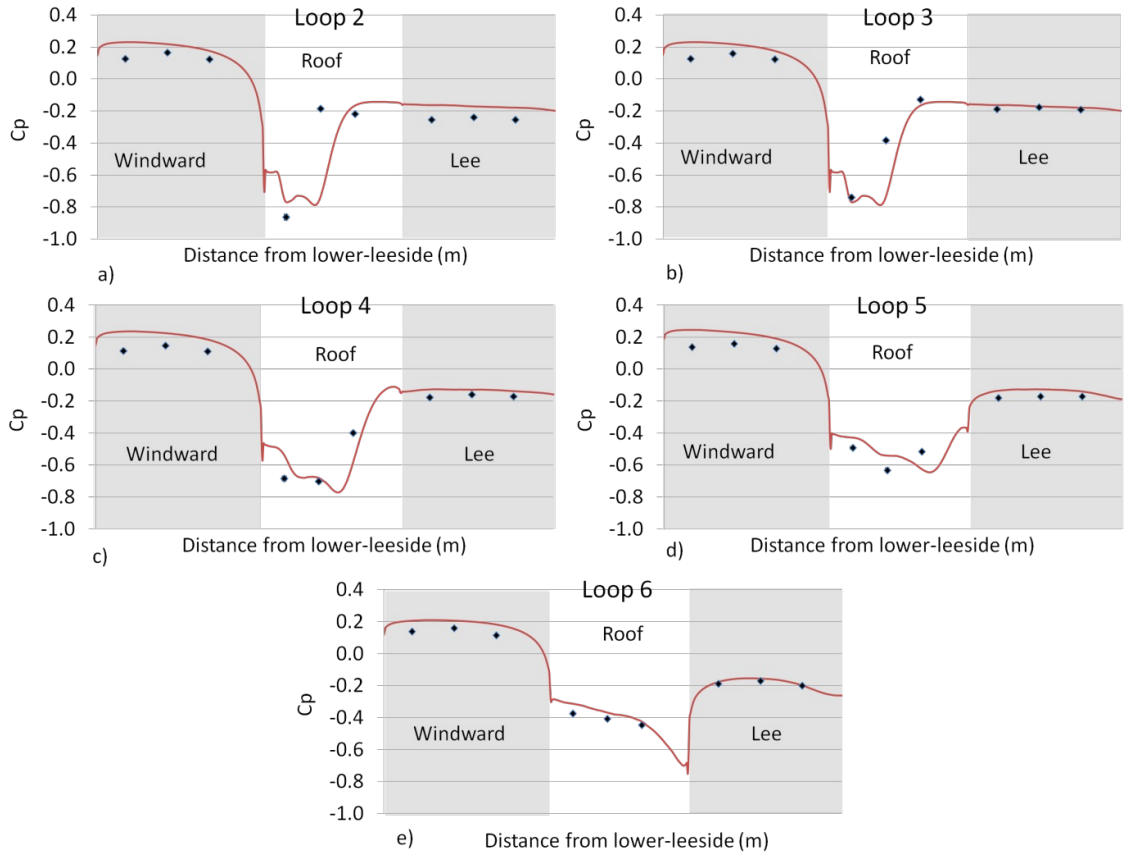

Figure 10 Time and ensemble-averaged surface pressure coefficients from numerical simulations and physical experiments (Soper, 2014)

The comparison between the numerical and experimental C_ps on the third container are shown in Figure 10. The largest discrepancy between the numerical and experimental data occurs at the closest tapping loop to the leading edge of the container. This is because the leading edge is dominated by separation which can be affected by interference effects from the preceding container but also by the freestream turbulence of the CWG. The turbulence intensity and length-scale of an incident wind has been shown to affect the surface pressures on ground vehicles (Robinson and Baker, 1990, Baker and Humphreys, 1996, García et al., 2015) with the above effects considered, the agreement between the results presented in Figure 10 is deemed to be adequate.

6.3 Time-averaged flow

6.3.1 Velocity magnitudes on the windward side of the train

The simulations use a train-fixed frame of reference with a moving ground plane which has been widely used in train aerodynamics simulations (Bowman, 2005, Flynn et al., 2014, Huang et al., 2014, Pii et al., 2014). By setting the boundary conditions this way the flow can be simulated around a moving object without the need for using sliding mesh techniques which can greatly increase the complexity of a case.

The focus of the current work is the effect of slipstream gusts on people at trackside, thus it is important that the velocity is considered in the frame of reference of a static observer. The normalised velocity magnitude, U, is converted to the frame of reference of a static observer by

$$U = \frac{\sqrt{(u - u_{train})^2 + v^2 + w}}{u_{train}} \qquad (2)$$

where u, v, and w are longitudinal, lateral and vertical velocity components within the computational domain, respectively. The positions of slipstream flow property sampling are shown in Figure 11 and are used on either side of the train for the windward and leeward samples.

Time-averaged velocity magnitudes from samples at y=1.59 m, y=1.84 m, y=2.34 m and y=3.34 m are considered for the no-crosswind, 10º and 30º crosswind cases. These lateral positions correspond to 0.25 m, 0.5 m, 1 m and 2 m from train side. The flow variables in the slipstream will be considered at three different heights above TOR, namely z=0.5 m, z=2 m and z=4 m.

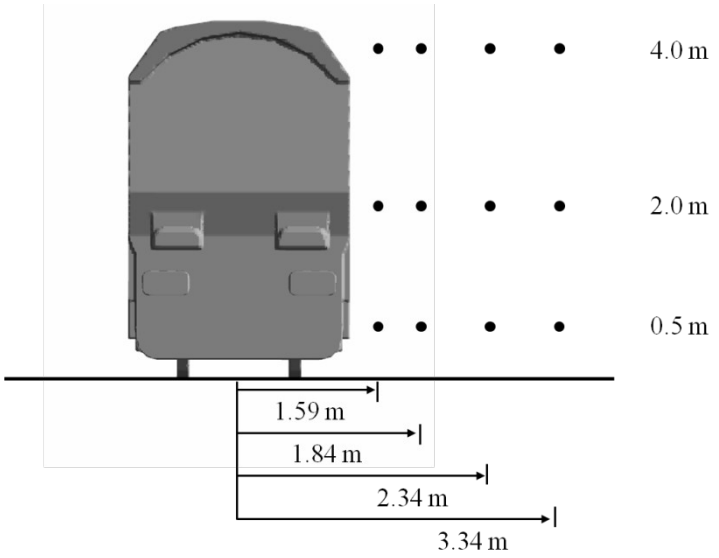

Figure 11 Positions of slipstream sampling relative to TOR and COT

The velocity magnitudes on the windward side of the train for the no-crosswind, 10° and 30°crosswind cases at z=0.5 are shown in Figure 12. In the no-crosswind case the highest peak velocities are U=0.95 and U=0.76 at y=1.59 m and y=1.84 m, respectively. The peak slipstream velocity in the no-crosswind case is lower than the crosswind in the 30° case at y=2.34 m and y=3.34 m. At all positions from COT the velocity in the 30° case decreases in the nose region due to the flow stagnating on the train. The velocity continues to decrease along train length and is punctuated by velocity transients at inter-wagon spacings. The velocity from the no-crosswind case in the boundary layer region is greater than in the 10º and 30º cases from y=1.59 m to y=2.34 m although at y=3.34 m the velocity in the 30° case is greatest, due to the reduced effect of stagnation at that distance from COT. The velocity in the 10° case exhibits nose peaks at y=1.59 m and y=1.84 m, which are greater than the crosswind velocity ahead of the train, and are caused by the flow separating around the windward corner of the locomotive.

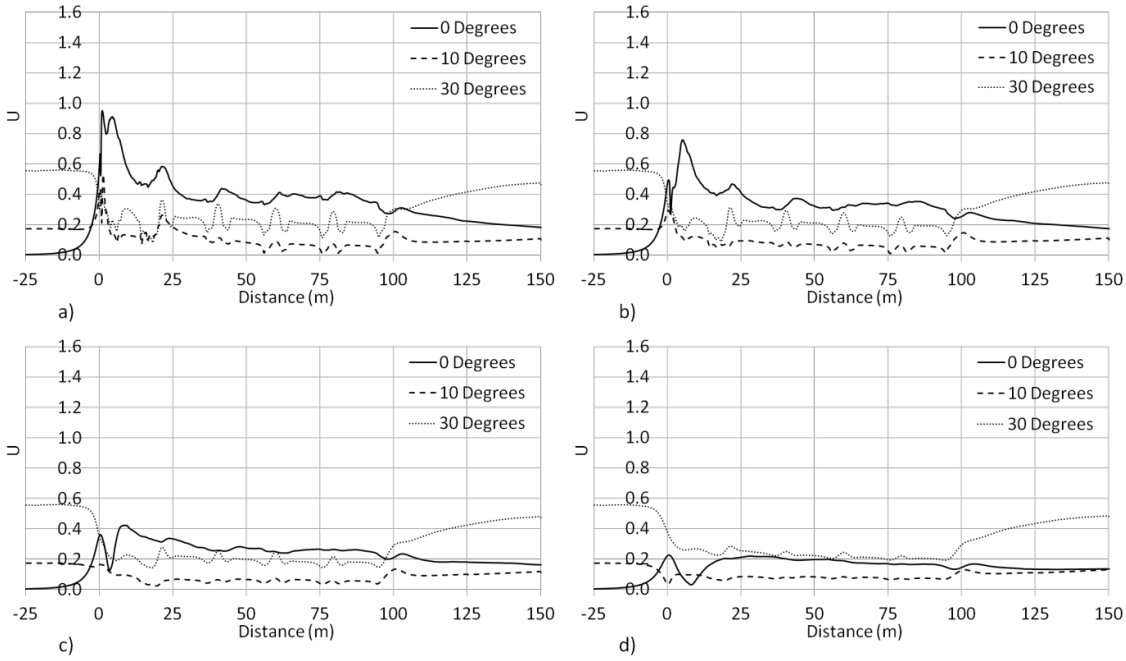

Figure 12 Time-averaged slipstream velocity magnitude on the windward side of the train at z= 0.5 m for a) y=1.59 m, b) y=1.84 m c) y=2.34 m, d) y=3.34 m for the no-crosswind (Flynn et al., 2014), 10° and 30° crosswind cases

The velocity magnitude on the windward side of the train at z=2m is shown in Figure 13. At y=1.59 m, the velocity nose peaks for the no-crosswind and 10° cases are greater than the crosswind velocity of the 30° case. In the boundary layer region the velocities for all the cases are reasonably comparable for y=1.59 m and y=1.84 m, however only the 30° case exhibits transients of approximately ΔU=0.2. The velocity from the 30° case is nearly double the no-crosswind and 10° cases at y=3.34 m.

The magnitudes of the transients in the boundary layer region of the 30° case are greater than the velocity in the boundary layer region of the no-crosswind case. At $x \approx 100$ m, the velocity increase in the 30° case is approximately ΔU=0.2, whereas the transients for the no- and 10° crosswind cases are less than half of this value. The velocity from the 30° case at y=3.34 m is greater than the velocity for the n-crosswind and 10° crosswind cases for the entirety of train length.

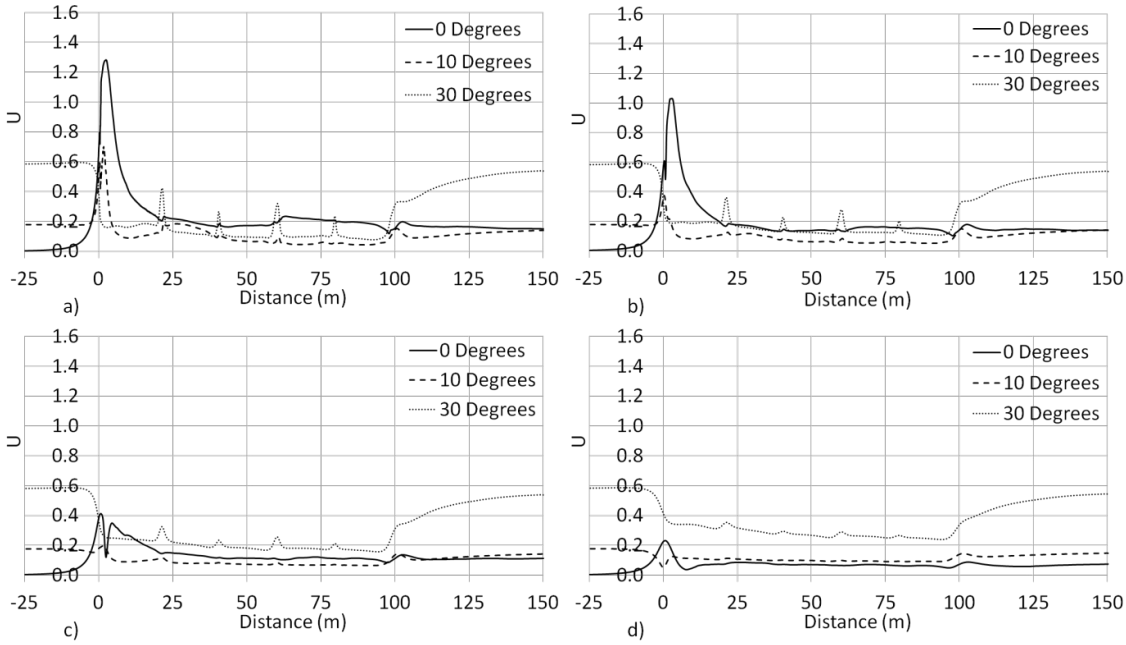

Figure 13 Time-averaged slipstream velocity magnitude on the windward side of the train at z= 2 m for a) y=1.59 m, b) y=1.84 m c) y=2.34 m, d) y=3.34 m for the no-crosswind (Flynn et al., 2014), 10° and 30° crosswind cases

At z=4 m the velocity in the boundary layer region of the 30° case is greater than its crosswind velocity for the first height above TOR (Figure 14). The velocity from the 10° case is greater than the no-crosswind case in the first half of the boundary layer region at y=1.59 m, and for the entire boundary layer region at all other distances from COT. Higher velocities occur at z=4 m than have previously been seen for the 10° and 30° cases because of flow separation over the roof of the containers. This is enhanced for the 30° case due to the greater lateral component of the crosswind than in the 10° case which causes more abrupt flow separation, lower pressure and thus higher velocities to occur.

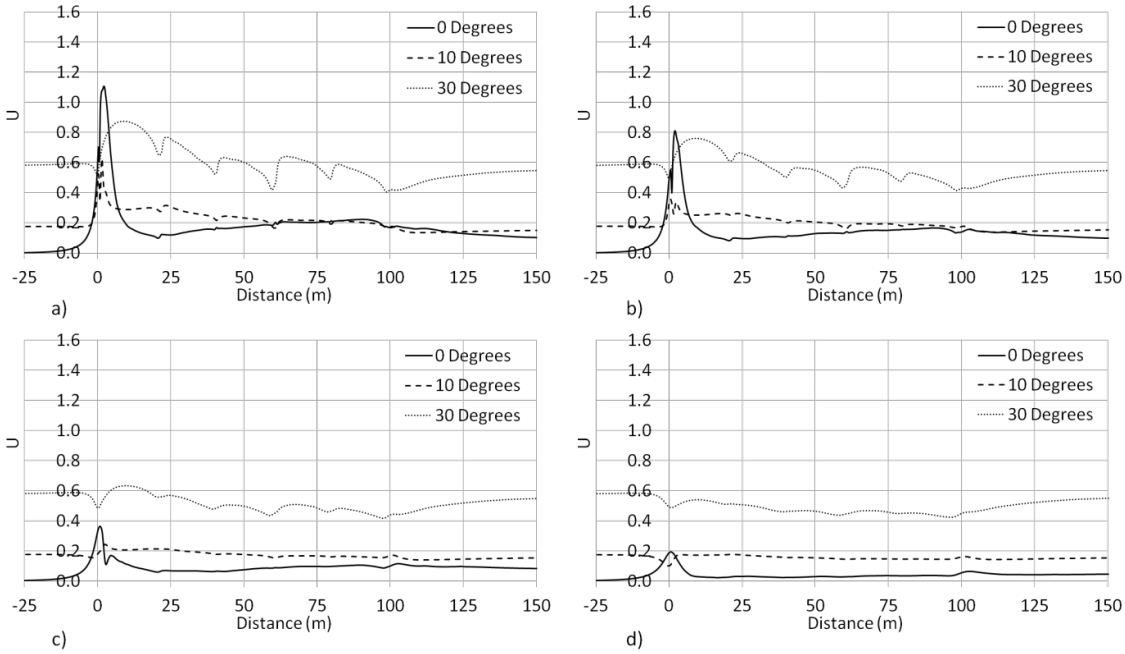

Figure 14 Time-averaged slipstream velocity magnitude on the windward side of the train at z= 4 m for a) y=1.59 m, b) y=1.84 m c) y=2.34 m, d) y=3.34 m for the no-crosswind (Flynn et al., 2014), 10° and 30° crosswind cases

6.3.2 Velocity magnitude on the leeward side of the train

Figure 15 shows the velocity magnitude on the leeward side of the train at z=0.5 m. On the leeward side of the train, at y=1.59 m and z=0.5 m, the nose region velocities of both crosswind cases are within 30% of the no-crosswind peak. A double velocity peak is visible for all cases, which becomes more accentuated with increasing yaw angle. With increasing distance from train side the difference between the velocities in the nose region becomes more pronounced such that the no-crosswind velocity is observed to decrease fastest with distance from train side, followed by the 10º case and then the 30º case. In the boundary layer region, at y=1.59 m and y=1.84 m, the no-crosswind case has the greatest velocity followed by the 10° case and then the 30° case which is a result of the shielding effect. The peak velocities on the leeward side of the 30° case which occur at y=2.34 m and y=3.34 m have values twice those of the crosswind velocity. At y=3.34 m the peak velocity of the 10° case is greater than four times the velocity of its crosswind and the peak of the no-crosswind case.

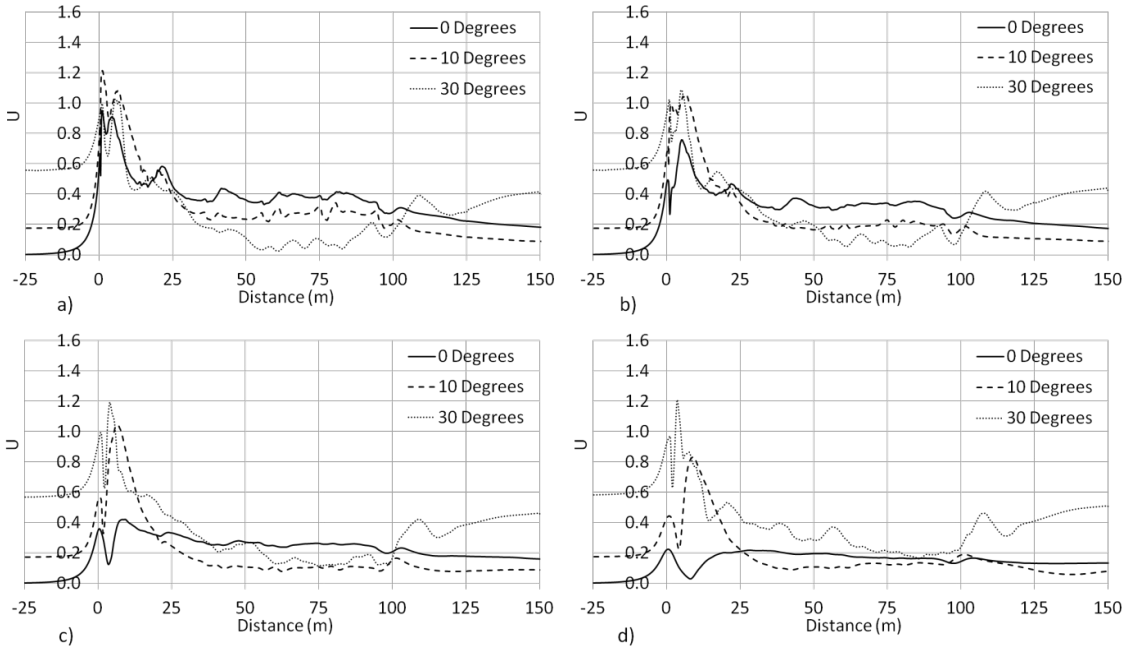

Figure 15 Time-averaged slipstream velocity magnitude on the leeward side of the train at z= 0.5 m for a) y=1.59 m, b) y=1.84 m c) y=2.34 m, d) y=3.34 m for the no-crosswind (Flynn et al., 2014), 10° and 30° crosswind cases

Figure 16 shows velocity magnitudes on the leeward side of the freight train at z=2 m. A significant variability in velocity is observed along train length for the 30º case in comparison to the no-crosswind and 10º crosswind cases. This is due to the larger lateral velocity component which causes additional air to pass through the inter-wagon spacings which then accelerates around the leeward front corners of the container wagons. The largest transient at an inter-wagon spacing is approximately $\Delta U=1.0$ which is twice magnitude the velocity transient which occurs at y=1.84 m.

The velocity peak in the nose region of the 30º case differs by less than 13% between y=1.59 m and y=3.34 m due to the presence of a shear layer which extends further from train side than in the 10º case because of the higher yaw angle (Figure 17).

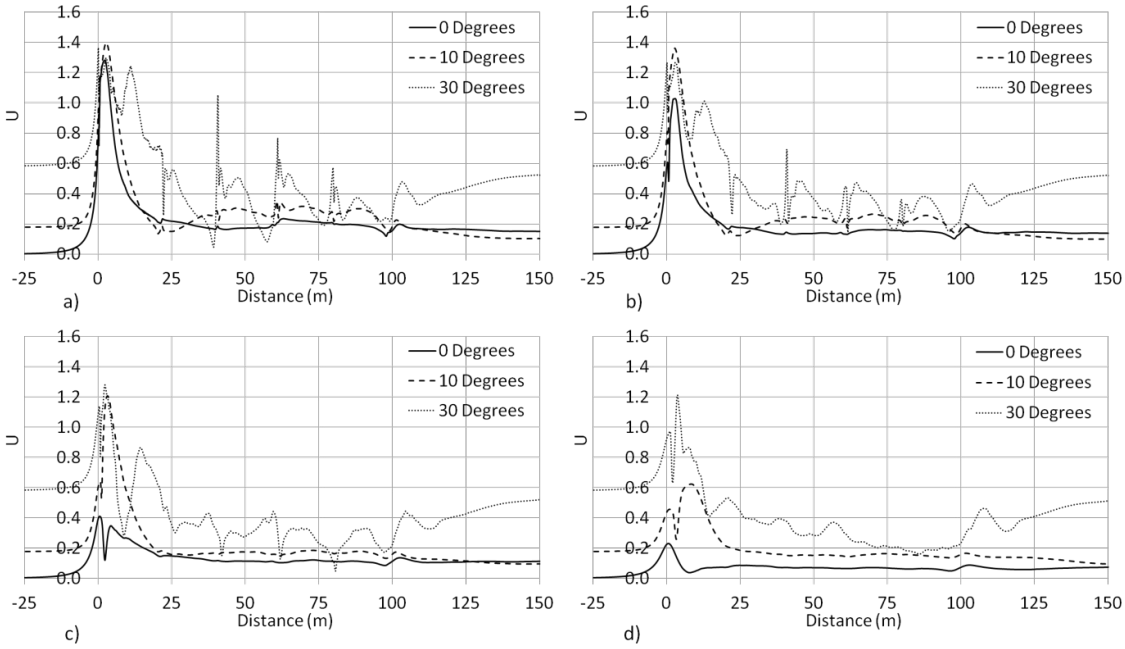

Figure 16 Time-averaged slipstream velocity magnitude on the leeward side of the train at z=2 m for a) y=1.59 m, b) y=1.84 m c) y=2.34 m, d) y=3.34 m for the no-crosswind (Flynn et al., 2014), 10° and 30° crosswind cases

The 10º crosswind case shows increasing velocity after the locomotive at y=1.59 m and y=1.84 m whereas at further distances from train side the velocity remains nearly constant after *x*=30 m. This increase in velocity is a result of the low pressure region on the leeward side of the train 'pulling' the air along with it.

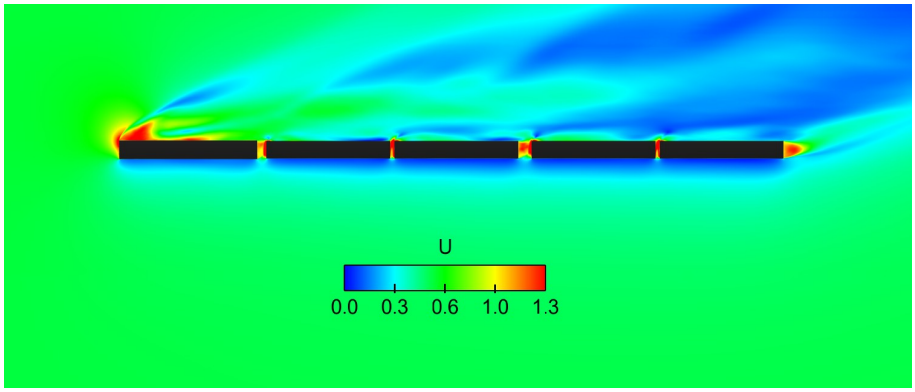

Figure 17 Colour plot of velocity magnitude, U, on a plane at z=2 m in the 30° crosswind case

Figure 18 shows the velocity magnitude on the leeward side of the train at z=4 m. The mean velocity magnitudes from the 10º and 30º crosswind cases are greater than those obtained from the no-crosswind case for the majority of train length at all distances from COT. The higher velocities from the crosswind cases are a result of the flow separating around the leeward front corners of the containers and over the roofs causing higher lateral and vertical components in comparison to the no-crosswind case where the longitudinal component is dominant.

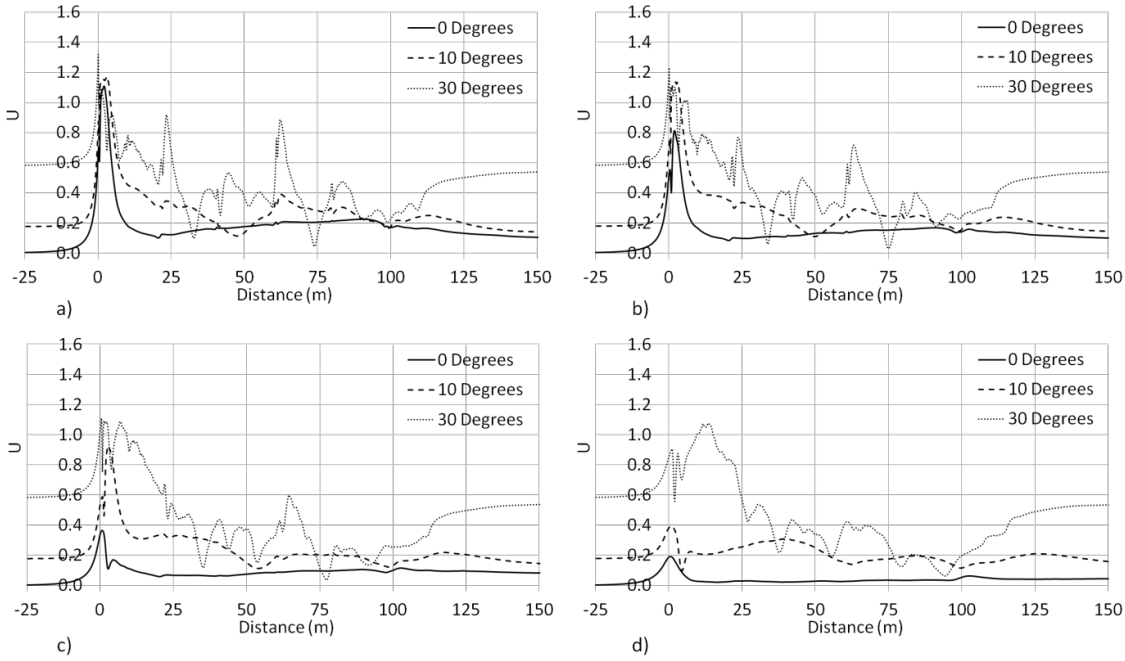

Figure 18 Time-averaged slipstream velocity magnitude on the leeward side of the train at z=4 m for a) y=1.59 m, b) y=1.84 m c) y=2.34 m, d) y=3.34 m for the no-crosswind (Flynn et al., 2014), 10° and 30° crosswind cases

6.3.3 Comparison of freight train slipstream to high speed train slipstream

The slipstream of a model-scale ICE2 was investigated using the University of Birmingham's TRAIN rig (Baker et al., 2001). As well as measuring the slipstream velocities of the train in ambient conditions, the vehicle was also passed through a crosswind and the slipstream velocity on the leeward side was measured using hot-wire anemometers. Comparison between the present work and Baker et al.,(2001) is made in order to highlight the different effects that crosswinds have on the slipstreams of freight

and passenger trains. It should be noted that the yaw angle considered by Baker et al., (2001) was 11º although due to unsteadiness in the crosswind generator and variation of train speeds between runs some variability will arise in the ensemble average. Baker et al., (2001) only measured the longitudinal and lateral velocity components hence Figure 19 shows the normalised horizontal velocities at y'=1m and y'=2 m on the leeward sides of the trains. The normalised horizontal velocity, U_h, is the normalised velocity magnitude, U, without the vertical component (w=0). The model-scale ICE2 is comprised of four cars and is 100 m long which matches the train in the current case

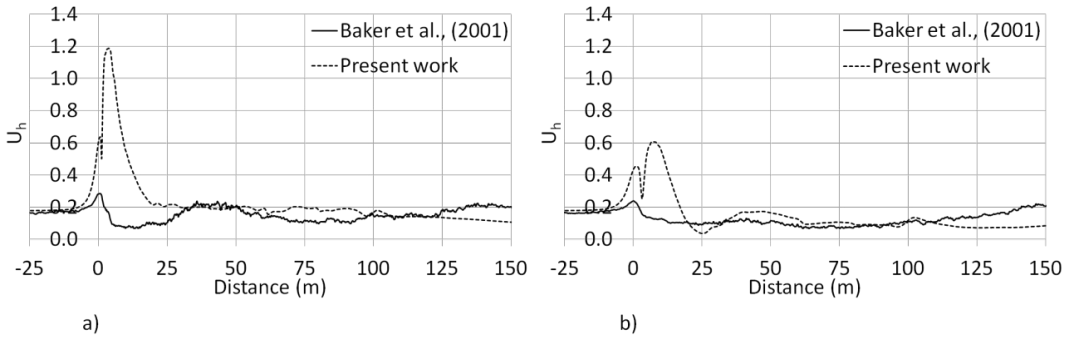

Figure 19 Time-averaged and ensemble-mean normalised horizontal slipstream velocities, U_h, on the leeward side of the freight train in the present work and the ICE2 (Baker et al., 2001) at a) 1 m and b) 2m from train side at z=2.25 m

At y'=1 m the greatest difference in velocities from the two cases occurs in the nose region of the trains. The peak velocity on the leeward side of the ICE2 is 0.28, whereas it is 1.19 on the leeward side of the Class 66 locomotive. The relatively massive nose peak from the present work has been attributed to the flow shearing around the corners of the locomotive whereas the relatively low U_h on the leeward side of the ICE2 is due to the rounded shape which prevents such abrupt flow separation.

Further from train side, at y'=2 m, the peak velocity generated by the Class 66 is 0.6 which is half the peak value at y'=1 m. The peak velocity in the slipstream of the ICE2, at y'=2 m, is 0.24, 40% of the peak velocity on the leeward side of the Class 66.

The velocities from Figure 19 are presented as absolute values in Figure 20. It should be noted that the ICE2 used in (Baker et al., 2001) travels at approximately 80 m/s, even so, the freight train produces higher slipstream velocities for a much lower crosswind speed. At y'=2 m, the freight train still produces the greatest slipstream velocity even though the crosswind is half the speed of that in the passenger train case.

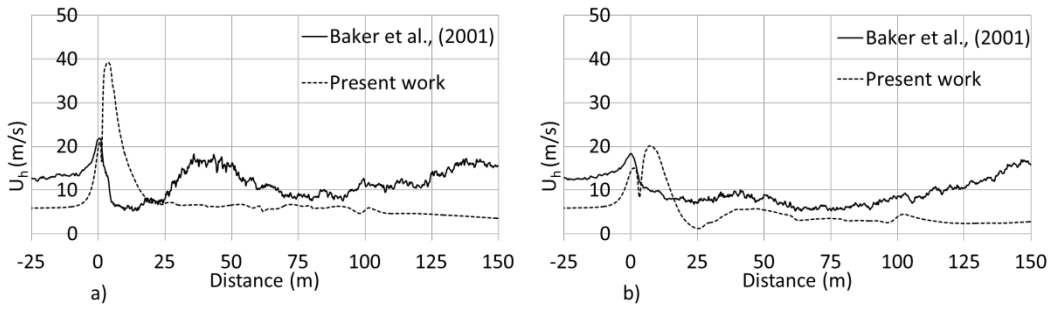

Figure 20 Time-averaged and ensemble-mean absolute horizontal slipstream velocities, U_h, on the leeward side of the freight train in the present work and the ICE2 (Baker et al., 2001) at a) 1 m and b) 2m from train side at z=2.25 m

6.4 Instantaneous flow

6.4.1 Instantaneous peak velocities

It was demonstrated in Section 6 that the slipstream velocities generated on the windward side of a train which is subjected to a crosswind are minimal in comparison to those on the leeward side. To this end only the instantaneous velocities on the leeward side of the train will be considered here. The velocities shown in Figure 21 are maximum values from samples along a line in the computational domain at 20 independent time-steps, as was done in Flynn et al., (2014) and is the closest equivalent of a train passing a static observer that in possible with a fixed model in CFD.

With increasing distance from train side the mean peak velocity in the no-crosswind case decreases from 1.49 at y=1.59 m to 0.7 and 0.45 at y=2.34 m and y=3.34 m, respectively. At y=1.59 m and y=1.84 m, the 10° mean peak velocity remains fairly constant and then decreases significantly at y=2.34m and y=3.34 m. The mean peak

velocities for the 30° case are seen to remain relatively constant for all measurement distances from train side as a result of the position of the shear layer generated by the incident wind.

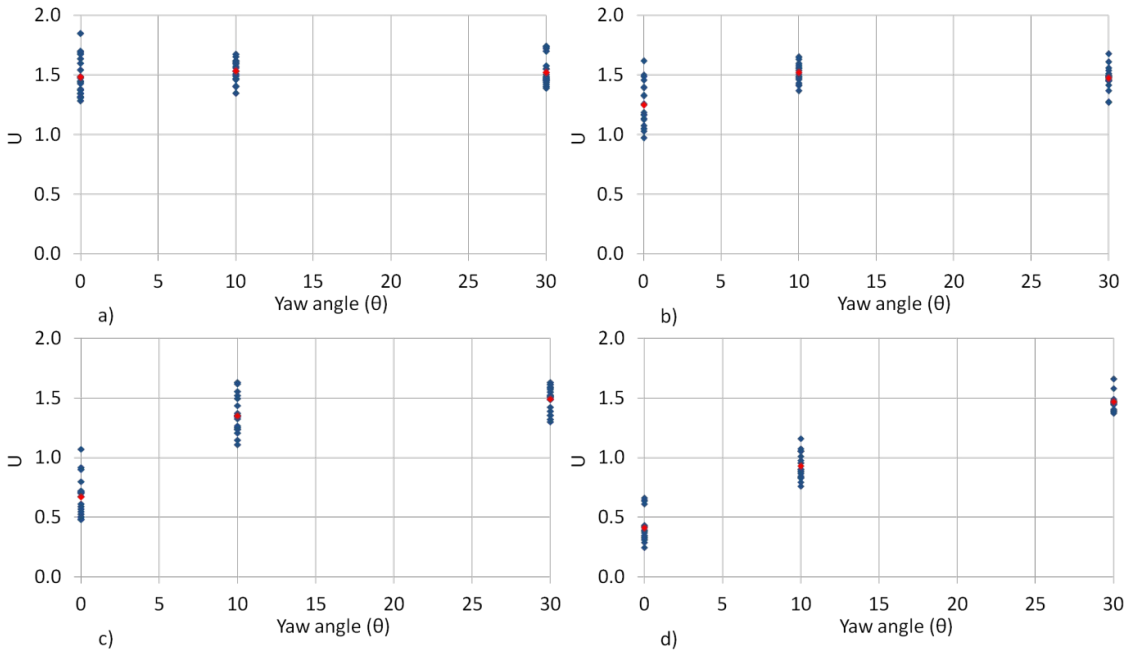

Figure 21 Instantaneous peak velocity magnitudes relative to a static observer for each yaw angle case at z=2 m and a) y=1.59 m, b) y=1.84 m, c) y=2.34 m and d) y=3.34 m. Red indicates the mean of the instantaneous peaks.

The spread of the peak velocities is seen to be dependent on the yaw angle and position from the train. The standard deviation of the velocities in the no-crosswind case decrease with distance from COT as a result of the sampling location being outside of the unsteady flow separation region around the front of the locomotive, see Flynn et al., (2014). The standard deviation for the 10° case reaches its greatest value at y=2.34 m as a result of the position of the unsteady shear layer.

At all distances from COT the no-crosswind case has the highest standard deviation with its peak being σ_u=0.18 and occurring at y=1.84 m.

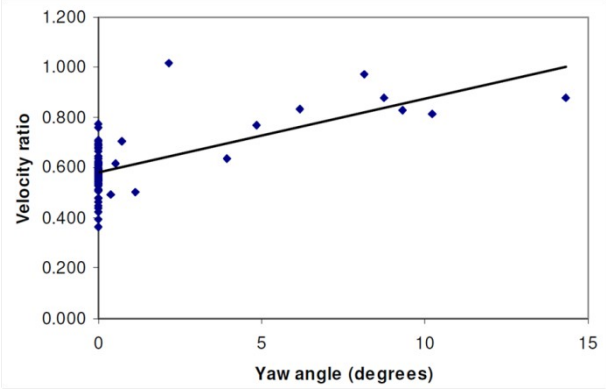

Figure 22 Instantaneous peak velocities against resultant yaw angle relative to freight trains at z=1 m (lateral position unknown) (Baker et al., 2007)

The velocities presented in Figure 21 bare strong resemblance to those which were obtained at full-scale and given in Baker et al., (2007) shown in Figure 22. The velocities from the numerical simulations have set yaw angle values whereas in the full-scale data, yaw angles are approximated from local wind speeds and train speed causing more scatter in the full-scale data than in the numerical data. However, the near-linear correlation is very similar to that shown from the current work even though the full-scale data only show 13 measurements with crosswind.

7. Stability of people subjected to gusts

The data presented above show slipstream amplification around the freight train and in order to give a practical dimension to the results, they are used as inputs into a mathematical model of person stability. The following section presents the methodology and results from using the velocities as inputs to a previously-developed spring-mass-damper model and shows the safety implications of slipstream amplification.

7.1 Theory

The wind-induced force experienced by a standing person can be approximated by (Penwarden et al., 1978)

$$F(t)=\frac{1}{2}\rho A_p C_d \qquad 1$$

where A_p is the projected area to the wind and C_d is the drag coefficient. Estimating the projected area of a given person to the wind can be performed using the Dubois area, A_{DU}, (Du Bois and Du Bois, 1916) which is calculated as

$$A_{DU}=0.0769\, W_p^{0.425} h_p^{0.725} \qquad 2$$

where W_p is the weight of a person in Newtons and h_p is the height of a person in metres. The Dubois area is a convenient parameter for approximating the projected area of a person based upon easily obtainable parameters such as height and weight. The validity of the exponents were verified by Penwarden et al.,(1978) for a sample size of 331 and were found to be suitable.

Penwarden et al.,(1978) used wind tunnel testing to evaluate the drag force experienced by persons standing in a wind tunnel. Clothing was found to have a significant effect of forces on persons, as a result of the change in projected area. The orientation of a person to an oncoming wind also has a strong effect on the force on a person due to the difference in projected area. The drag coefficients for a person facing the wind and a person side-on to the wind are 1.17 and 1.01, respectively.

It was noted by Fukuchi (1961) that a person subjected to a gust has a response time of approximately 0.375 s in which they behave as a solid object due to the speed at which the muscles react. The response of a human to a wind-induced force during the first 0.375 s can be crudely approximated as a cuboid (Figure 23) (Johnson and Prevezer, 2005).

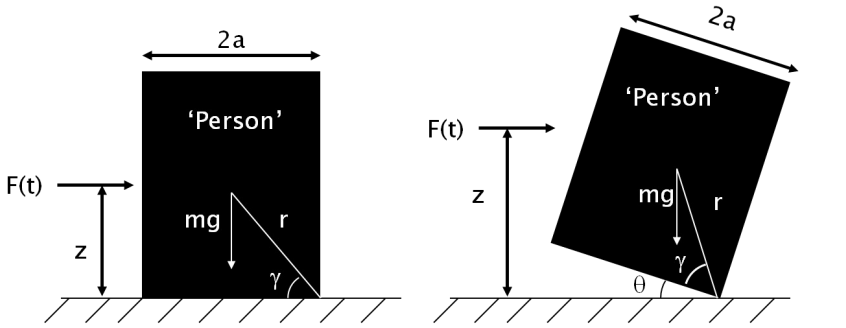

Figure 23 Cuboid subjected to a wind-induced load in original and displaced positions

The cuboid model has the advantage of being very simple to implement although it is a gross simplification of human reaction to gusts. Furthermore, the cuboid model is only considered to be valid for 0.375 s after a young or middle-aged person is exposed to a gust, this value is 0.476 s for elderly people (Mackey and Robinovitch, 2006).

Perhaps a more realistic method of approximating the dynamic behaviour of the human body in its reaction gusts is the spring-mass-damper system developed by Jordan (2008); the schematic of the model is shown in Figure 24. In the model, the human body is considered to consist of three masses moving relative to one another which represent the motion of the legs, torso and head, of a person with springs and dampers to represent the elastic behaviour of the muscles (Wexler et al., 1997). The displacement of the cuboid model at t=0.375 s is used as the initial displacement of the spring-mass-damper model.

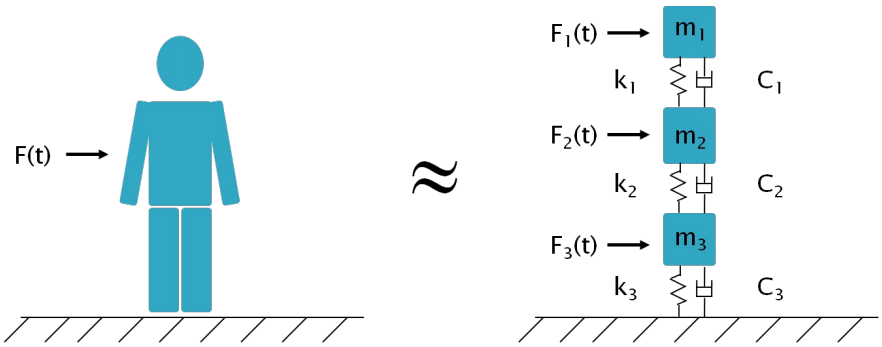

Figure 24 Schematic of the spring-mass-damper stability model of a person

The spring-mass-damper model relies on constants in order to calibrate its behaviour to something akin to the response of a person subjected to a wind-induced force. In order to calibrate the modal constants Jordan et al.,(2008) placed 29 volunteers in a wind tunnel and measured their response to different step change gusts

The model randomly generates 100 people with different height and weight characteristics that are in line with the population and also randomly-selects their orientation. For full details of the model and the wind tunnel test procedure see Jordan (2008).

In order to simulate a wind-induced force on the person stability model, input velocities were required. Each randomly-generated person was subjected to one of 20 instantaneous velocities sampled from the simulations, those from the no-crosswind, 10° and 30° crosswind case are shown in Figure 25.

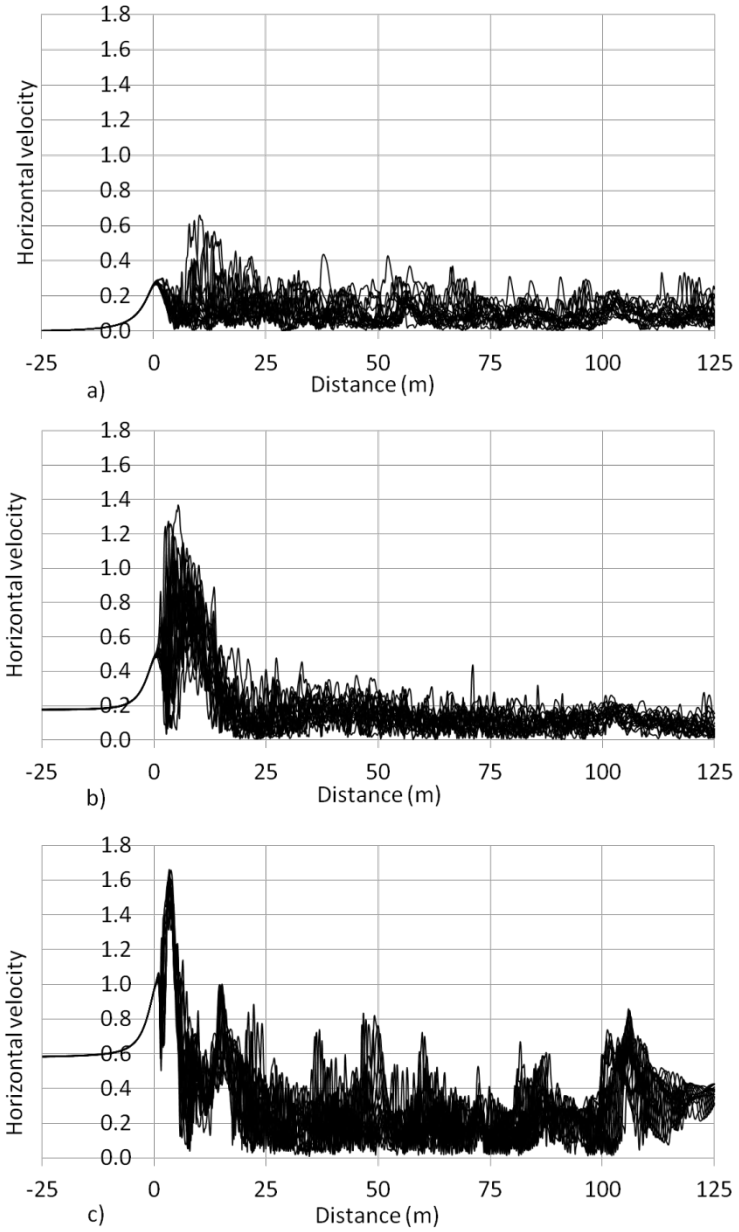

Figure 25 Horizontal velocities from the leeward side of the train at y=3 m and z=2m for the a) no-crosswind, b) 10° crosswind and c) 30° crosswind cases

Figure 26 shows slipstream velocities from the no-crosswind case juxtaposed against a velocity time series from wind tunnel experiments detailed in Jordan et al., (2008). The slipstream velocities exhibit impulse gusts in the form of a dominant peak and show good resemblance to the step input of the wind tunnel tests. This difference between the velocities from the numerical and wind tunnel work is not likely to be significant because it is the initial gust which is responsible for person unsteadiness and once the

wind stabilises about the free stream then the person will have already reacted to the gust and will hence be braced.

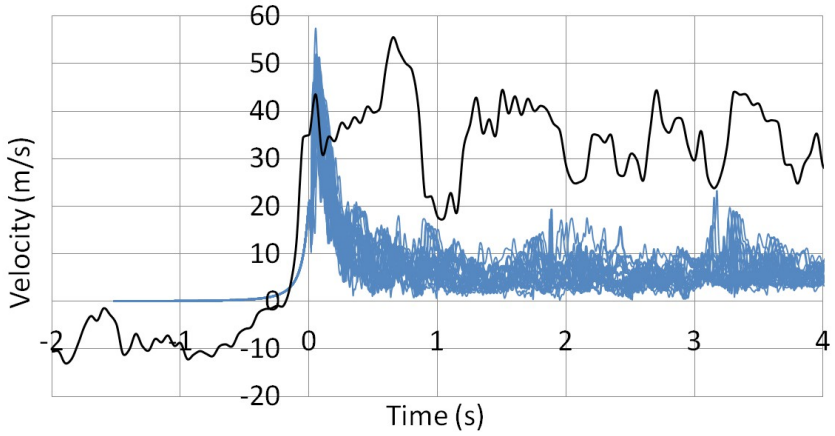

Figure 26 Twenty instantaneous velocities from no-crosswind simulations (blue) and velocity from Jordan et al., (2008). Wind tunnel velocities are scaled to be comparable to slipstream velocities.

In this work the randomly-generated people were subjected to one of 20 instantaneous velocities obtained from the CFD simulations, unlike in Jordan (2008) where the velocities were unique for each person tested. It is assumed that applying the velocities from the CFD simulations to a randomly-generated person is the same as applying a unique randomly-generated velocity to randomly-generated people. The basis of this assumption is that the velocities obtained from the simulations are numerous enough to provide a representative sample of the range of velocities which occur in a slipstream.

The velocities sampled from the numerical simulations possess some physical basis, however the assumption is made that the velocities next to a static vehicle at a single instant in time are the same as those measured by a static probe when a train passes.

The slipstream velocities were sampled at z=2 m which, assuming a platform height of z=1 m, gives velocities at approximately mid-height of a person although it is also

assumed that the presence of the platform has a negligible effect on the slipstream velocity.

Velocities closer than y=2 m have been neglected due to potentially misleading results because it is considered highly unlikely that a person would stand 1 m closer to the train than the yellow safety line especially considering the audible warnings and platform attendants present at stations. The furthest position of slipstream sampling was chosen as y=4 m because this was at the outer portion of the high-resolution mesh region and solution validity of samples at further distances from train side cannot be assured.

Figure 27 shows a distribution of the heights and weights of 1000 randomly-generated people from the model. The distribution is superficially comparable to that obtained by Penwarden et al.,(1978), therefore it can be considered that the heights and weights of the randomly-generated people used in the model are reasonable and thus sufficient for the purposes of the present work.

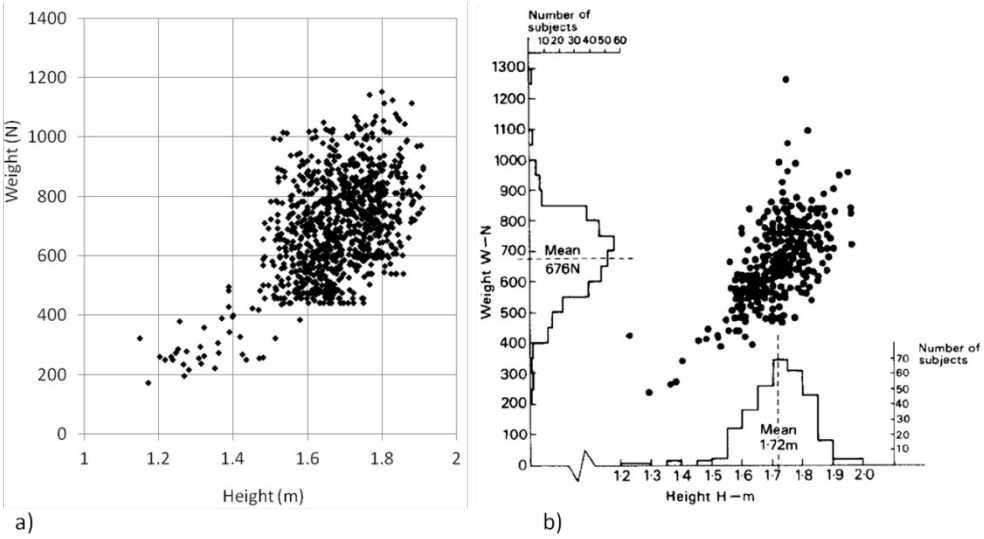

Figure 27 Comparison of the distribution of the heights and weights of a) randomly-generated people in the mathematical spring-mass-damper model and b) people used in wind tunnel experiments (Penwarden et al., 1978)

7.2 Stability model results

The results from the spring-mass-damper model model are presented in Table 1. The data refer to the percentage of person unsteadiness caused by the slipstream gusts at each position relative to train side.

The model was run three times at each measurement position and each crosswind in order to ensure that the results were repeatable and that the data from a single run did not give inaccurate data. The results from the spring-mass-damper model were tested and for three runs produced person unsteadiness values within 3 % of each other.

The probability of person instability caused by velocities sampled between y=2 m and y=4 m for the no-crosswind, 10º and 30º crosswind cases is shown in Table 1. The no-crosswind case produces no person instability at y=4 m whereas the 10º and 30º crosswinds cause instabilities rates of 35 and 54 %, respectively. Between the 10º and 30º cases, the likelihood of person unsteadiness increases by 54 % which is consistent with the trend of the peak slipstream velocities as shown in Figure 22.

Table 1 Person instability results for velocities obtained between y=4 m and y=2 m from centre of track at z=2 m

	Percentage person unsteadiness caused by slipstream velocities		
Distance from COT (m)	**No crosswind**	**10 crosswind**	**30 crosswind**
4.0	0	35	54
3.5	0	46	79
3.0	0	64	97
2.5	7	85	84
2.0	34	96	97

At y=3 m, the likelihoods of person unsteadiness for the 10° and 30° crosswinds are 64 % and 97 %, respectively whereas the likelihood of a person becoming unsteadied by a slipstream gust in the no-crosswind case is 0%. These results appear reasonable considering that yellow lines on station platforms are situated at y=2.95 m and there are no reports of a person becoming unsteadied on the UK rail network standing at this position.

Closer to the train side, at y=2.5 m, the likelihood of a person becoming unsteadied in ambient conditions increases to 7.2 % from 0 % at y=3 m. A negligible increase in person unsteadiness is observed for the 30° case, and the percentage of people displaced by the slipstream in the 30° case is less than the 10° case for the first time. At y=2 m, the probabilities of person unsteadiness caused by the slipstreams are 34, 96 and 97 % for the no-crosswind, 10° and 30° crosswind cases, respectively.

Figure 28 collates data from Table 1 in order to show the effect of distance from train side on the likelihood of a person becoming unsteadied in each crosswind scenario. For the no-crosswind case the risk is shown to be negligible at y=3 m which gives credence to the yellow safety line on station platforms. The level of person unsteadiness in the 10º crosswind case exhibits a near-linear decrease with distance from COT whereas the 30º case reaches a peak at y=3 m and then decreases at a slightly higher rate.

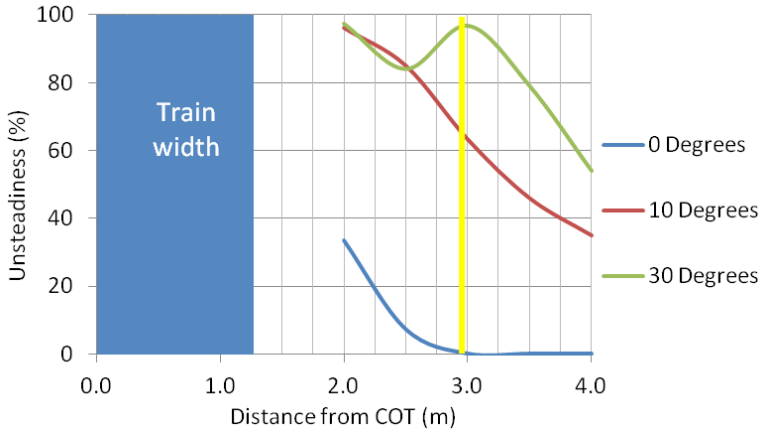

Figure 28 Percentage chance of person instability against distance from train side for the no-crosswind, 10º and 30º crosswind cases, yellow line is positioned at y=2.95 m

If it is assumed that the percentage unsteadiness for the 10º crosswind case decreases at the same rate as shown in Figure 28, then the position of 0 % person instability will occur at y=5.1 m. Not all station platforms extend up to y=5 m therefore, for the majority of platform scenarios, the occurrence of a 10º crosswind on a Class 66 locomotive-hauled container freight train will cause some person unsteadiness. The effective width of a platform can be reduced when large numbers of passengers are waiting which can cause people to stand closer to train side than would otherwise be the case and therefore have the potential to increase the risk of person unsteadiness.

Jordan (2008) found the probability of person instability at 1.5 m from centre of track caused by a freight train travelling at 30 m/s through a station was 22 %. In the present case, only 7 % instability is observed 0.34 m closer to the train. Jordan (2008) based the freight train slipstream model around measurements obtained on a platform at y'=1.5 m from a British Class 92 with 46 partially loaded container wagons in tow. Fully-loaded consists, such as the one used in the present case, have been shown to produce lower slipstream velocities than partially-loaded consists (Soper, 2014). Therefore it is anticipated that the slipstream of the no-crosswind case is less likely to cause person instability, which explains the discrepancy between the data.

The speed of the crosswind from the 30° case is approximately 16.5 m/s. From the literature regarding person instability, it can be considered likely that a person would have difficulty standing in such a high wind and hence the question of whether slipstream amplification causes instability is somewhat muted. Further, at such wind speeds it is unlikely that freight trains would operate due to the risk of container shedding.

The case modelled in this work is an idealised scenario and does not take into account local infrastructure such as station buildings. Local infrastructure is likely to reduce wind speeds which cause the data presented here to be a conservative estimate of risk and open the subject of crosswind subjected slipstream to further investigation.

8. Conclusions

This paper presented results from numerical simulations of flow field around a model-scale freight train subjected to two different crosswinds as well as the person instability probabilities caused. From the data presented the following conclusions are drawn:

- Lower pressures and higher velocities were observed on the leeward side of the train in crosswind conditions than on the windward side
- Velocity nose peaks are rarely observed on the windward side of the train except at 1.59 m and 1.84 m from the centre of track in the 10° yaw angle case.
- The greatest inter-wagon transients for both pressure and velocity occur in the 30° yaw angle case on both sides of the train.
- Significantly different flow regimes are observed for the three different heights above TOR on both the windward and leeward sides of the train.
- The freight train shows significantly more slipstream amplification for a lower crosswind speed than a high speed passenger train produced for a much higher crosswind speed.

- Although slipstream amplification is significant in the 30° yaw angle case, the speed of crosswind required is 16.5 m/s, which is well within ranges which are considered to be dangerous to person stability.

- No person instability is observed in the no-crosswind case at 3 m from the centre of track and is in line with observations on the UK rail network.

- The 30° yaw angle case causes high levels of person instability for all measurement positions on the leeward side of the train.

References

ALAM, F. & WATKINS, S. 2007. Effects of Crosswinds on Double Stacked Container Wagons. *16th Australasian Fluid Mechanics Conference, 2-7 December.* Gold Coast, Australia.

BAKER, C. J., DALLEY, S. J., JOHNSON, T., QUINN, A. D. & WRIGHT, N. G. 2001. The slipstream and wake of a high-speed train. *Proceedings of the Institution of Mechanical Engineers, Part F: Journal of Rail and Rapid Transit,* 215**,** 83-99.

BAKER, C. J. & HUMPHREYS, N. 1996. Assessment of the adequacy of various wind tunnel techniques to obtain aerodynamic data for ground vehicles in cross winds. *Journal of Wind Engineering and Industrial Aerodynamics,* 60**,** 49-68.

BAKER, C. J., QUINN, A., SIMA, M., HOEFENER, L. & LICCIARDELLO, R. 2013a. Full-scale measurement and analysis of train slipstreams and wakes. Part 2 Gust analysis. *Proceedings of the Institution of Mechanical Engineers, Part F: Journal of Rail and Rapid Transit*.

BAKER, C. J., QUINN, A. D., SIMA, M., HOEFENER, L. & LICCIARDELLO, R. 2013b. Full-scale measurement and analysis of train slipstreams and wakes: Part 1 Ensemble averages. *Proceedings of the Institution of Mechanical Engineers, Part F: Journal of Rail and Rapid Transit*.

BAKER, C. J., STERLING, M., JOHNSON, T., FIGURA-HARDY, G. I. & POPE, C. W. The effect of crosswinds on train slipstreams. International Conference on Wind Engineering, 2007 Cairns, Australia.

BELL, J. R., BURTON, D., THOMPSON, M., HERBST, A. & SHERIDAN, J. 2014. Wind tunnel analysis of the slipstream and wake of a high-speed train. *Journal of Wind Engineering and Industrial Aerodynamics,* 134**,** 122-138.

BELL, J. R., BURTON, D., THOMPSON, M. C., HERBST, A. H. & SHERIDAN, J. 2015. Moving model analysis of the slipstream and wake of a high-speed train. *Journal of Wind Engineering and Industrial Aerodynamics,* 136**,** 127-137.

BOUFERROUK, A., HARGREAVES, D. & MORVAN, H. 2012. CFD Simulations of Crosswind Impinging on a High Speed Train Model.

BOWMAN, I. 2005. Saftey of Slipstream Effects Produced by Trains: Pilot CFD Analysis of the Effect of Crosswinds on Train Slipstreams. Report Prepared by Mott McDonald for Project RSSBT425 Saftey of slipstreams produced by trains.

BOWMAN, J. 2015. 'It was a tragic accident': Toddler killed when pram sucked onto tracks by high-speed train. *The Mirror,* 29/04/2015.

DEEG, P., JÖNSSON, M., KALTENBACH, H., SCHOBER, M. & WEISE, M. 2008. Cross-comparison of measurement techniques for the determination of train induced aerodynamic loads on the track bed. *Proc. BBAA VI.* Milano, Italy.

DIEDRICHS, B. 2003. On computational fluid dynamics modelling of crosswind effects for high-speed rolling stock. *Proceedings of the Institution of Mechanical Engineers, Part F: Journal of Rail and Rapid Transit,* 217**,** 203-226.

DIEDRICHS, B., SIMA, M., ORELLANO, A. & TENGSTRAND, H. 2007. Crosswind stability of a high-speed train on a high embankment. *Proceedings of the Institution of Mechanical Engineers, Part F: Journal of Rail and Rapid Transit,* 221**,** 205-225.

DU BOIS, D. & DU BOIS, E. F. 1916. A formula to estimate the approximate surface area if height and weight be known. *Nutrition (Burbank, Los Angeles County, Calif.),* 5**,** 303.

FLYNN, D., HEMIDA, H., SOPER, D. & BAKER, C. 2014. Detached-eddy simulation of the slipstream of an operational freight train. *Journal of Wind Engineering and Industrial Aerodynamics,* 132**,** 1-12.

FUKUCHI, G. 1961. Field Measurements of Train Drafts. *Permanent Way,* 4.

GARCÍA, J., MUÑOZ-PANIAGUA, J., JIMÉNEZ, A., MIGOYA, E. & CRESPO, A. 2015. Numerical study of the influence of synthetic turbulent inflow conditions on the aerodynamics of a train. *Journal of Fluids and Structures,* 56**,** 134-151.

GOLOVANEVSKIY, V. A., CHMOVZH, V. V. & GIRKA, Y. V. 2012. On the optimal model configuration for aerodynamic modeling of open cargo railway train. *Journal of Wind Engineering and Industrial Aerodynamics,* 107–108**,** 131-139.

HEMIDA, H. & BAKER, C. J. 2010. Large-eddy simulation of the flow around a freight wagon subjected to a crosswind. *Computers & Fluids,* 39**,** 1944-1956.

HEMIDA, H., BAKER, C. J. & GAO, G. 2012. The calculation of train slipstreams using Large-Eddy Simulation. *Proceedings of the Institution of Mechanical Engineers, Part F: Journal of Rail and Rapid Transit,* 228**,** 25-36.

HEMIDA, H. & KRAJNOVIC, S. 2005. Large-Eddy Simulation of the flow around a simplified high speed train under the influence of a cross-wind. *17th AIAA Computational Fluid Dynamics Conference.* Toronto, Canada.

HUANG, S., HEMIDA, H. & YANG, M. 2014. Numerical calculation of the slipstream generated by a CRH2 high-speed train. *Proceedings of the Institution of Mechanical Engineers, Part F: Journal of Rail and Rapid Transit***,** 1–14.

JOHNSON, T. & PREVEZER, T. 2005. Mechanical model of human loss of balance due to wind gusts. *EACWE4 – The Fourth European and African Conference on Wind Engineering.* Prague, Czech Republic.

JORDAN, S., C. 2008. *An investigation of the slipstreams and wakes of trains and the associated effects on trackside people and objects.* PhD, The University of Birmingham.

JORDAN, S. C., JOHNSON, T., STERLING, M. & BAKER, C. J. 2008. Evaluating and modelling the response of an individual to a sudden change in wind speed. *Building and Environment,* 43**,** 1521-1534.

MACKEY, D. C. & ROBINOVITCH, S. N. 2006. Mechanisms underlying age-related differences in ability to recover balance with the ankle strategy. *Gait & posture,* 23**,** 59-68.

MULD, T. W., EFRAIMSSON, G. & HENNINGSON, D. S. 2013. Wake characteristics of high-speed trains with different lengths. *Proceedings of the Institution of Mechanical Engineers, Part F: Journal of Rail and Rapid Transit*.

PENWARDEN, A. D., GRIGG, P. F. & RAYMENT, R. 1978. Measurements of wind drag on people standing in a wind tunnel. *Building and Environment,* 13**,** 75-84.

PII, L., VANOLI, E., POLIDORO, F., GAUTIER, S. & TABBAL, A. 2014. A full scale simulation of a high speed train for slipstream prediction. *Proceedings of the Transport Reserach Arena, Paris, France*.

PIOMELLI, U. 2008. Wall-layer models for large-eddy simulations. *Progress in Aerospace Sciences,* 44**,** 437-446.

POPE, C. 2006. Safety of Slipstreams Effects Produced by Trains. A report prepared by Mott Macdonald Ltd for railway safety and standards board. 2 ed. Mott MacDonald, Croydon.

QUINN, A. D., BAKER, C. J., STERLING, M., SIMA, M., WEISE, M., HOEFENER, L. & EISENLAUER, M. 2011. The Effect of Crosswinds on the Slipstreams of High Speed Trains. *In:* C GUERTS, T., EDITOR (ed.) *The 13th international conference on wind engineering*. Amstrerdam, The Netherlands.

ROBINSON, C. G. & BAKER, C. J. 1990. The effect of atmospheric turbulence on trains. *Journal of Wind Engineering and Industrial Aerodynamics,* 34**,** 251-272.

SOPER, D. 2014. *The aerodynamics of a container freight train.* PhD thesis, University of Birmingham.

SOPER, D., BAKER, C. & STERLING, M. 2014. Experimental investigation of the slipstream development around a container freight train using a moving model facility. *Journal of Wind Engineering and Industrial Aerodynamics,* 135**,** 105-117.

STERLING, M., BAKER, C. J., C., J. S. & T., J. 2008. A study of the slipstreams of high-speed passenger trains and freight trains. *Proceedings of the Institution of Mechanical Engineers, Part F: Journal of Rail and Rapid Transit,* 222**,** 177-193.

SWEBY, P. K. 1984. High resolution schemes using flux limiters for hyperbolic conservation laws. *SIAM journal on numerical analysis,* 21**,** 995-1011.

TAGES ANZEIGER. 2015. Einjähriger stirbt nach Unfall mit Güterzug. *(In German)*.

TSI 2008. Relating to the 'Rolling Stock' Sub-System of the Trans-European High-Speed Rail System, 2008/232/CE. *Official Journal of The European Union*.

WEXLER, A. S., DING, J. & BINDER-MACLEOD, S. A. 1997. A mathematical model that predicts skeletal muscle force. *Biomedical Engineering, IEEE Transactions on,* 44**,** 337-348.